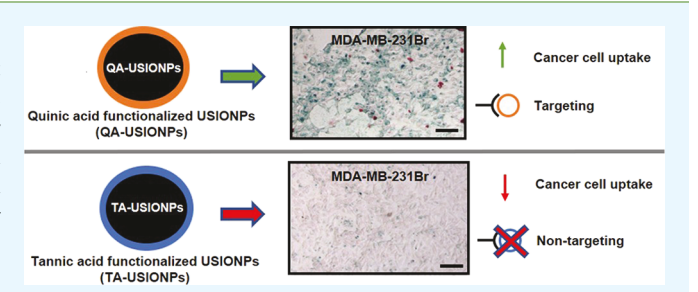


Role of Surface Chemistry in Mediating the Uptake of Ultrasmall Iron Oxide Nanoparticles by Cancer Cells

Akshay A. Narkhede, Jennifer A. Sherwood, Angelo Antone, Kasie R. Coogan, Mark S. Bolding, Sanghamitra Deb, Yuping Bao, And Shreyas S. Rao

Supporting Information

ABSTRACT: Ultrasmall iron oxide nanoparticles (USIONPs) (<4 nm) have recently attracted significant attention because of their potential as positive T_1 magnetic resonance imaging (MRI) contrast agent contrary to larger superparamagnetic iron oxide nanoparticles (>6 nm) which act as negative T_2 MRI contrast agents. However, studies on the cellular uptake behavior of these nanoparticles are very limited compared to their counterpart, larger-sized superparamagnetic iron oxide nanoparticles. In particular, the effects of specific nanoparticle parameters on the cellular



uptake behavior of USIONPs by various cancer cells are not available. Here, we specifically investigated the role of USIONPs' surface functionalities [tannic acid (TA) and quinic acid (QA)] in mediating cellular uptake behavior of cancer cells pertaining to primary (U87 cells) and metastatic (MDA-MB-231Br cells) brain malignancies. Here, we chose TA and QA as representative capping molecules, wherein TA coating provides a general negatively charged nontargeting surface while QA provides a tumortargeting surface as QA and its derivatives are known to interact with selectin receptors expressed on tumor cells and tumor endothelium. We observed differential cellular uptake in the case of TA- and QA-coated USIONPs by cancer cells. Both the cell types showed significantly higher cellular uptake of QA-coated USIONPs compared to TA-coated USIONPs at 4, 24, and 72 h. Blocking studies indicated that P-selectin cell surface receptors, in part, mediated the cellular uptake of QA-coated USIONPs. Given that P-selectin is overexpressed in cancer cells, tumor microenvironment, and at the metastatic niche, QA-coated USIONPs hold potential to be utilized as a platform for tumor-targeted drug delivery and in imaging and detection of primary and metastatic tumors.

KEYWORDS: cancer targeting, ultrasmall iron oxide nanoparticles, quinic acid, tannic acid, P-selectin

1. INTRODUCTION

Ultrasmall iron oxide nanoparticles (USIONPs) (<4 nm) have recently attracted considerable attention because of their ability to act as a biocompatible positive T_1 magnetic resonance imaging (MRI) contrast agents. The ability to perform as a positive T_1 MRI contrast agent renders USIONPs highly valuable in disease monitoring; particularly in cancer diagnosis and imaging. Conventionally, in a clinical setting, gadolinium complexes are used as T_1 MRI contrast agents which produce a brighter MRI image with high resolution resulting in easy detection. 1,2 However, gadolinium complexes are known to cause brain lesions because of undesirable accumulation in addition to acute liver and kidney toxicity.^{1,3} To overcome the toxicity associated with gadolinium complexes, larger superparamagnetic iron oxide nanoparticles (diameter typically greater than 6 nm) (e.g., Feridex) were approved by U.S. food and drug administration (FDA) as negative T2 MRI contrast agents owing to their biocompatibility.^{1,4} However, they were later taken off of the market because of the low resolution and high background interference. 1,2,5 In addition, they tend to passively accumulate in the liver, spleen, and lymph nodes which further limit their efficacy in imaging diseased tissue. 1,6,7 USIONPs have the potential to overcome these challenges associated with both gadolinium complexes and larger superparamagnetic iron oxide nanoparticles by acting as the biocompatible T_1 MRI contrast agent.^{8,9} In addition to serving as the T_1 MRI contrast agent, USIONPs can also be engineered to specifically target tumor cells. Tumor-targeting ligands and chemotherapeutic drugs can be simultaneously conjugated to the USIONPs surface in order to deliver chemotherapeutic drugs in a targeted manner, hence demonstrating their potential as a therapeutic platform. 10 Therefore, in addition to imaging, USIONPs can be

Received: January 10, 2019 Accepted: April 24, 2019 Published: April 24, 2019



[†]Department of Chemical and Biological Engineering, The University of Alabama, Tuscaloosa, Alabama 35487, United States

^{*}Department of Radiology, The University of Alabama at Birmingham, Birmingham, Alabama 35233, United States

[§]Central Analytical Facility, The University of Alabama, Tuscaloosa, Alabama 35487, United States

simultaneously utilized as a targeted drug carrier, making them excellent candidates for cancer theranostics. 10

In general, for the nanoparticles to be effective for cancer targeting applications, the uptake of nanoparticles by cancer cells is critical. Several factors influence cellular uptake of nanoparticles in vitro and in vivo. 11,12 These include physicochemical factors such as the size, shape, surface charge, and surface chemistry. ^{11–17} For instance, the shape and size of nanoparticles influence the cellular uptake by governing the way the nanoparticles bind and activate the cell membrane for uptake. 11,18–21 In addition, surface charge of the nanoparticles also influences the cellular uptake by mediating the surface protein adsorption which impacts the nanoparticle-cell membrane interactions. 11,22 Apart from the physical aspects, surface chemistry also plays a key role in mediating cellular uptake, which can be altered by coating or functionalizing the nanoparticle surface with biocompatible polymers. For example, larger superparamagnetic iron oxide nanoparticles coated with biocompatible polymers like poly-L-lysine,² polyethylene glycol,²⁴ poly vinyl alcohol,²⁵ chitosan,²⁵ and carbohydrates like dextran,²⁶ amino-dextran,²⁶ and starch²⁴ have been designed to passively target cancer cells through tumor accumulation, selective tumor embolization, or by enhanced permeability and retention effect.²⁷ To specifically target cancer cells, larger superparamagnetic iron oxide nanoparticles have also been engineered to actively interact with cancer cell-specific membrane receptors through monoclonal antibodies, 28-44 small peptides, or molecules. 45 However, compared to the well-understood larger superparamagnetic iron oxide nanoparticles (utilized as T2 MRI contrast agent), 46-49 the impact of physicochemical properties of USIONPs on the cellular uptake behavior of cancer cells needs further investigation.

Previously, we demonstrated the shape-dependent cellular uptake in case of positive T_1 spherical tannic acid (TA)-coated USIONPs (TA-USIONPs) and TA-coated ultrasmall nanowires, wherein we found that the uptake of spherical TA-USIONPs by HepG2 liver cells was much higher (26%) compared to TA-coated US nanowires (5%). 50 In the present study, we investigated how the surface chemistry of USIONPs impacts the cellular uptake by characterizing and comparing the uptake of quinic acid (QA)-coated USIONPs (QA-USIONPs) by cancer cells pertaining to highly aggressive primary and metastatic brain malignancies to that of TA-USIONPs in vitro. QA was chosen as QA and its derivatives have been known to interact with the P-selectin cell surface receptors^{51–53} which is overexpressed in tumor cells,^{54–56} tumor microenvironment,^{56,57} and at the metastatic niche.^{56,58–60} We investigated the differences between the cellular uptake of QA-USIONPs and TA-USIONPs and examined the role of P-selectin in mediating the selective uptake of QA-USIONPs.

2. MATERIALS AND METHODS

- 2.1. Materials. All of the chemical reagents were purchased and used without further purification, including chloroform (Sigma-Aldrich, 99%), acetone (BDH, 99.5%), ethanol (BDH, 100%), methanol (Alfa Aesar, 100%), TA (Acros, 95%), D-QA (Sigma-Aldrich, 98%), and 4-(2-hydroxyethyl)-1-piperazineethanesulfonic acid (HEPES, OmniPur).
- 2.2. Synthesis of QA-USIONPs and TA-USIONPs. Thermal decomposition of the iron oleate precursor to form USIONPs was used according to previously published papers. 9,50,61 Because the particles were synthesized under organic conditions, a modified ligand

exchange procedure⁹ was used to exchange the organic ligands on the as-synthesized USIONPs with either TA or QA. More specifically, either TA (15 mg, 0.008 mmol) or QA (70 mg, 0.36 mmol) was first dissolved in 0.5 mL of DI water followed by the addition of 5 mL of methanol and 5 mL of acetone. The solution was sonicated to mix well. Next, the cleaned and weighed USIONPs in chloroform (5 mL, 1 mg/mL) were added to the ligand solution and sonicated to mix well. The solutions were mixed overnight at 45 °C in a shaker at 250 rpm. Next, the particles were collected via centrifugation (15 min, 15 000 rpm) and redispersed in ethanol (5 mL) at a concentration of 1 mg/mL. An equal volume of water was added, and the solutions were heated up to evaporate the ethanol. The particles were finally collected via centrifugation and redispersed in water (5 mL) for a final concentration of 1 mg/mL. The particles were washed thrice with a 2:1 mixture of ethanol and water to remove excess TA or QA. For cell treatment, the QA/TA-USIONPs were sterilized in 70% ethanol for 15 min, collected via centrifugation, and redispersed in autoclaved 10 mM HEPES buffer at a final concentration of 1 mg/mL.

- 2.3. Characterization of QA-USIONPs and TA-USIONPs. QA-USIONPs and TA-USIONPs were characterized for their physical and surface properties. Specifically, the size and shape of the particles were determined using transmission electron microscopy (TEM), the hydrodynamic size and zeta potential were determined using dynamic light scattering (DLS, Malvern Zetasizer), and the surface chemistry was determined using Fourier transform infrared spectroscopy (FTIR). T_1 and T_2 relaxation times for both the TA-USIONPs and QA-USIONPs were measured using Bruker minispec (Mq60).
- **2.4. Cell Culture.** MDA-MB-231Br, a brain metastasizing variant of the triple negative breast cancer line MDA-MB-231 was generously provided by Dr. Lonnie Shea (University of Michigan). MDA-MB-231Br cells were routinely maintained in Dulbecco's modified Eagle's medium (Sigma-Aldrich) supplemented with 10% fetal bovine serum (FBS) (VWR Life Science) and 1% penicillin-streptomycin and cultured in a 37 °C and 5% CO₂ environment. U87, a glioblastoma multiforme (GBM) cell line was generously provided by Dr. Yonghyun Kim (The University of Alabama). U87 cells were routinely maintained in Eagle's modified Essential medium(ATCC) supplemented with 10% FBS and 1% penicillin-streptomycin and cultured in a 37 °C and 5% CO₂ environment.
- 2.5. Cell Proliferation. MDA-MB-231Br or U87 cells were seeded onto a 96-well plate at a cell seeding density of 5000 cells/well and were allowed to adhere overnight. The spent media was then removed and 100 μ L of fresh media containing 50 μ g/mL of either QA-USIONPs or TA-USIONPs was added to each well (for dosedependent studies, concentration of QA-USIONPs or TA-USIONPs ranging from 0 to 150 μ g/mL was used). The cells were allowed to uptake nanoparticles for 72 h. MTS assay (CellTiter 96, Promega) was performed at the end of 72 h as per the manufacturer's protocol. Briefly, the spent media containing nanoparticles was replaced by fresh media followed by incubation with CellTiter 96 solution for 2 h. After the incubation, absorbance reading was taken at 490 nm using a Filtermax F5 multimode microplate reader (Molecular Devices). The absorbance readings in case of cells treated with QA-USIONPs and TA-USIONPs were then compared to those of the nontreated control group.
- 2.6. Prussian Blue Staining. MDA-MB-231Br or U87 cells were seeded onto glass bottom chamber slides at a cell seeding density of 5000 cells/well and were allowed to adhere overnight. The spent media was then removed and 100 μ L of fresh media containing 50 μ g/mL of either QA-USIONPs or TA-USIONPs was added to each well. The cells were then allowed to uptake nanoparticles for 4, 24, and 72 h respectively. The control group was included for every time point, wherein the cells were not treated with nanoparticles. At each time point, the spent media containing nanoparticles was removed and the cells were washed at least twice and then fixed using 4% paraformaldehyde (PFA) solution in phosphate-buffered saline (PBS). The fixed cells were stained using Prussian blue staining kit (Polysciences Inc.) as per the standard protocol. Briefly, the cells were treated with 1:1 solution of 4% hydrochloric acid (HCl) and potassium ferrocyanide for 30 min at 37 °C followed by a 1:1 solution

ACS Applied Materials & Interfaces

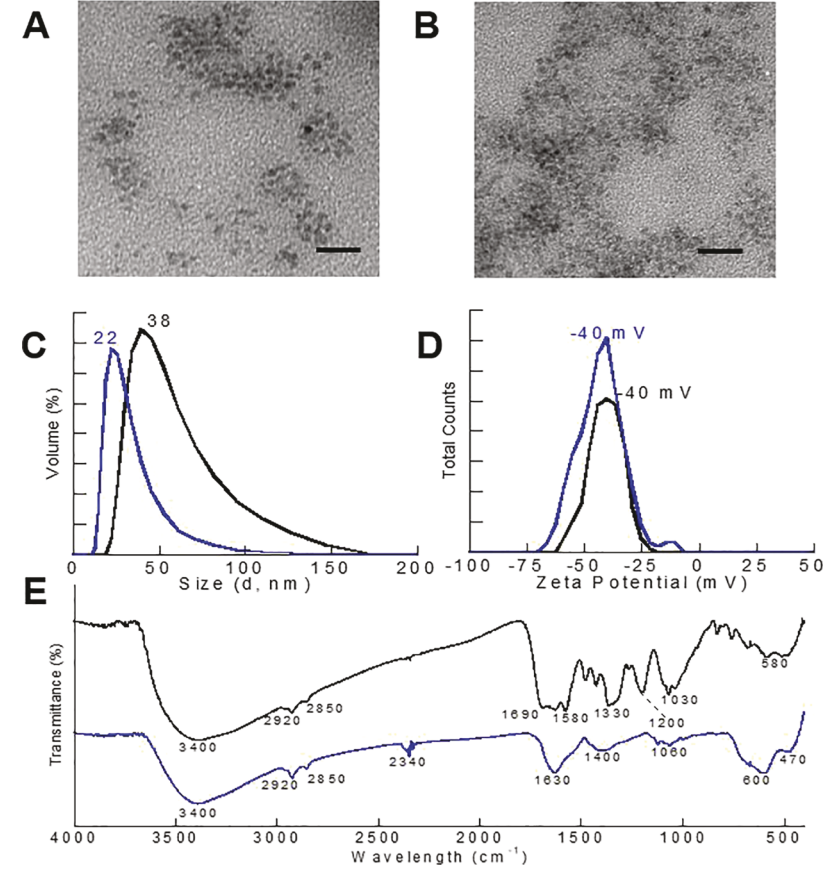


Figure 1. Characterization of TA-USIONPs and QA-USIONPs. TEM images of (A) TA-USIONPs and (B) QA-USIONPs (scale bar = 20 nm), (C) hydrodynamic size of TA-USIONPs and QA-USIONPs, (D) zeta potential of TA-USIONPs and QA-USIONPs, and (E) FTIR of TA-USIONPs and QA-USIONPs. TA is represented in black and QA in blue for all images.

of PBS and nuclear fast red dye for 5 min. The cells were washed (2×) and bright-field images were taken using an Olympus IX83 microscope.

2.7. Ferrozine Assay for Iron Quantification. To quantify the uptake of QA-USIONPs and TA-USIONPs by cancer cells and determine the intracellular iron concentration, ferrozine assay was performed as described previously. 62 Briefly, MDA-MB-231Br or U87 cells were seeded onto a 96-well plate at a cell seeding density of 5000 cells/well and were allowed to adhere overnight. The spent media was then removed and 100 μ L of fresh media containing 50 μ g/mL of either QA-USIONPs or TA-USIONPs was added to each well. The cells were allowed to uptake nanoparticles for 4, 24, and 72 h, respectively. The control group was included for every time point, wherein the cells were not treated with nanoparticles. The spent media containing nanoparticles was removed and the cells were washed with PBS (2x) at every time point. Further, the cells were lysed using 100 μ L per well of 50 mM NaOH solution in deionized nanopure water for 2 h at room temperature followed by overnight lysis at 4 °C. The lysate was then stored at 4 °C in Eppendorf tubes for iron quantification.

Cell lysates (100 μ L aliquots) were then placed in the Eppendorf tubes and 100 μ L of 10 mM HCl solution in deionized nanopure water was mixed followed by further addition of 100 μ L iron releasing solution (a freshly mixed 1:1 solution of 1.4 M HCl and 4.5% w/v KMnO₄ in deionized nanopure water). The mixture was then incubated at 60 °C for 2 h. The mixture was then allowed to cool to room temperature before adding 30 μ L of the iron-detection reagent (6.5 mM ferrozine, 6.5 mM neocuproine, 2.5 M ammonium acetate, and 1 M ascorbic acid dissolved in deionized nanopure water). After 30 min, 280 μ L of the solution was pipetted into a well of 96-well plate. The absorbance of the well was then measured at 562 nm on a microplate reader (Molecular Devices). The iron content was then

determined using the calibration curve generated through standard solutions of equal volumes. The standard solution for the calibration curve was made in the similar way by mixing 100 μL of FeCl $_3$ solution (0–20 $\mu g/mL$) in 10 mM HCl, 100 μL of 50 mM NaOH, 100 μL of releasing solution, and 30 μL of the iron detection reagent. In a separate experimental setup, we determined the number of cells per well in control, QA-USIONP-treated and TA-USIONP-treated groups at 4, 24, and 72 h, respectively, using the trypan blue exclusion test, which was then used to obtain iron content per cell at given time points.

2.8. Immunofluorescence Staining. MDA-MB-231Br or U87 cells were seeded onto a 96-well plate at a cell seeding density of 5000 cells/well and were cultured for 72 h. The spent media was then removed, and the cells were washed with PBS at least twice. The cells were then fixed using 4% PFA, permeabilized using 0.1% Triton-X (VWR) in PBS, and blocked with 5% bovine serum albumin in PBS. The cells were then incubated with 2.5 μ g/mL of the primary antibody (anti-P-selectin antibody) (sc-271267; Santa Cruz Biotechnology) overnight at 4 °C followed by incubation with 1 μ g/mL of the Alexa Fluor 488-conjugated goat anti-mouse secondary antibody for 2 h (Invitrogen). Cell nuclei were visualized using 4,6-diamidino-2-phenylindole (DAPI) (Invitrogen). Fluorescence images were taken using an Olympus IX83 microscope with a spinning disc confocal attachment.

2.9. Blocking Studies. MDA-MB-231Br cells were seeded onto a 96-well plate at a cell seeding density of 5000 cells/well and were allowed to adhere overnight. The spent media was then removed and 100 μ L of fresh media containing free QA (1.6, 16 and 160 μ g/mL) or anti-P-selectin antibody (2.5 and 16 μ g/mL) (sc-271267; Santa Cruz Biotechnology) was added to the wells. The cells were then incubated with free QA and anti-P-selectin antibody for 4 h before feeding them with 50 μ g/mL of QA-USIONPs. The cells were

allowed to uptake nanoparticles for 24 h, following which ferrozine assay was performed for iron quantification.

2.10. Statistical Analysis. All experiments were performed with at least n = 6 replicates per condition and the results are presented as mean ± standard deviation. For the comparison of two samples, a ttest was performed (using JMP software). For multiple comparisons, the acquired data were subjected to ANOVA followed by the post-hoc Tukey HSD test (using JMP software). In case of non-normal data, a nonparametric Wilcoxon each pair test was performed (using JMP software). P-value less than 0.05 was considered statistically significant.

3. RESULTS AND DISCUSSION

Here, we elucidated how TA and QA surface functionalities on USIONPs impact their uptake by cancer cells. TA coating provides a general negatively charged surface to USIONPs while QA was chosen because of its potential targeting ability as QA and its derivatives are known to interact with selectin receptors expressed on tumor cell surfaces.^{51–53} We demonstrated the targeting capability of QA-USIONPs by comparing their in vitro cellular uptake with the previously reported TA-USIONPs, 50,61 using highly aggressive primary (U87) and metastatic (MDA-MB-231Br) brain tumor cells as brainrelated malignances are extremely aggressive and current diagnostic as well as therapeutic techniques have proved largely ineffective in targeting these tumors. 63 Further, we investigated the differences between the cellular uptake of QA-USIONPs and TA-USIONPs; specifically, the role of P-selectin in mediating the selective uptake of QA-USIONPs.

3.1. Synthesis and Characterization of QA-USIONPs and TA-USIONPs. USIONPs (<4 nm) were synthesized using the well-defined thermal decomposition method. 9,50,61 For use in biological applications, a ligand exchange was performed to replace the organic ligands with biologically compatible molecules on the surface of USIONPs. Previously, we reported the synthesis of TA-USIONPs and also demonstrated their tumor-site accumulation in vivo. 50,61 TA was originally chosen as a surface ligand because of biocompatibility ^{64,65} and because the bulky nature of this hydrophilic molecule allowed for a hydrophilic environment and effective water exchange, necessary for use as a T₁ MRI contrast agent.⁶¹ In addition to biocompatibility, surface functionalization can be used to enhance cellular uptake by targeting cell surface receptors. Herein, we rationally functionalized the surfaces of USIONPs with QA to explore the potential of using QA to target cancer cells. We further evaluated the targeting potential of QA as a surface coating by comparing the cellular uptake of QA-USIONPs to TA-USIONPs.

To evaluate the USIONPs after the ligand exchange, both the QA-USIONPs and TA-USIONPs were characterized for their physical and chemical properties after the ligand exchange. The morphology and uniformity of TA-USIONPs and QA-USIONPs were evaluated using TEM. TEM imaging indicated that the TA-USIONPs (Figures 1A, S1A) and QA-USIONPs (Figures 1B, S1B) maintained their shape and size. The actual particle size after the ligand exchange was 2.5 ± 0.7 nm for TA-USIONPs and 3.0 \pm 0.7 nm for QA-USIONPs (Figure S1C,D).

To further characterize the bulk solution, DLS was used to determine the hydrodynamic size of the USIONPs (Figure 1C) after the ligand exchange. USIONPs prior to the ligand exchange had a hydrodynamic size of 5.5 \pm 1.7 nm. ⁵⁰ After the ligand exchange, the TA-USIONPs had a peak size of 38 ± 22 nm and the QA-USIONPs had a peak size of 22 \pm 14 nm. The

hydrodynamic size distribution was determined over an average of several (>10) measurements with a standard deviation as indicated above. The large hydrodynamic size increase and standard deviation for the TA-USIONPs and QA-USIONPs was likely because of interactions of the surface functional groups and counter ions present in solution, which is seen by the tail in the DLS plots (Figure 1C). The intensity and number distributions of TA-USIONPs and QA-USIONPs were also measured in culture media at 4, 24, and 72 h timepoints. A size increase at all time points was observed which might be due to the presence of serum in culture media (Figure S2A,B). DLS was also used to measure the USIONPs surface charge, and the zeta potential for both the QA-USIONPs and the TA-USIONPs (Figure 1D) was -40 mV. The highly negative zeta potential was indicative of the -OH surface functional groups and indicated good electrostatic repulsion.

FTIR was used to determine the surface chemistry of the TA-USIONPs and QA-USIONPs (Figure 1E). Both TA-USIONPs and QA-USIONPs exhibited broad -OH stretching at $3400~\text{cm}^{-1}$ as well as additional peaks for -OH bending vibration (1640 cm $^{-1}$), -OH bonding in plane (1330–1430 cm $^{-1}$), and out of plane (600–680 cm $^{-1}$). TA-USIONPs exhibited additional peaks characteristic of aromatic C=C stretching (1580 and 1485 cm⁻¹) and aromatic C-H out of plane bending (760 and 820 cm⁻¹). These peaks were not observed in the FTIR of OA-USIONPs. TA-USIONPs also exhibited the characteristic C-O peak at 1200 cm⁻¹ which may be indicative of partial oxidation. Finally, the characteristic peaks for carboxylic acid C=O stretching (1780–1710 cm⁻¹) were not observed on the IR for QA-USIONPs, indicating carboxylic acid interaction with the USIONPs surfaces.

We have previously shown that the surface capping molecules did not affect the magnetic response of the nanoparticles with high paramagnetic signal. 50,61 Here, the T_1 and T_2 relaxation times for both the TA-USIONPs and QA-USIONPs were measured using a Bruker minispec (Mq60). The characteristic relaxivities $(r_1 \text{ and } r_2)$ were calculated according to the following equation, $1/T_{i \text{ sample}} = 1/T_{i \text{ solvent}} +$ $r_i[M](i = 1,2)$, where $1/T_{i \text{ sample}}$ and $1/T_{i \text{ solvent}}$ are the relaxation times of USIONPs solutions and pure solvent in s^{-1} , respectively, [M] is the concentration of iron in mM, and $r_i(i = 1,2)$ is the relaxivity of the USIONPs. TA-USIONPs exhibited an r_1 of 2.8 mM⁻¹ s⁻¹, an r_2 of 6.4 mM⁻¹ s⁻¹, and an r_2/r_1 ratio of 2.3. QA-USIONPs had r_1 relaxivity of 1.1 mM⁻¹ s⁻¹, r_2 relaxivity of 6.3 mM⁻¹ s⁻¹, and an r_2/r_1 ratio 5.8.

The r_2/r_1 ratios are a key indicator to determine whether a contrast agent is suitable as a T_1 or T_2 contrast agent. Typically, a T_1 contrast agent has an r_2/r_1 ratio less than 4 and a T_2 contrast agent has an r_2/r_1 ratio greater than 10. Here, QA-USIONPs exhibited an r_2/r_1 ratio of 5.8 which is an indication that QA-USIONPs may be able to function as a dual T_1/T_2 contrast agent. The differences in the relaxivities and relaxivity ratios of the TA-USIONPs and QA-USIONPs were likely because of the surface coatings. We previously hypothesized that TA would make a good surface coating for T_1 contrast agents because the bulky sized molecule could allow for fast water exchange from the USIONP surfaces to the surroundings.⁵⁰ QA, a much smaller molecule, likely had very tight, dense ligand packing on the USIONP surfaces. Tightly packed ligand surfaces may inhibit water exchange and lower T_1 efficiency. The data further support this hypothesis as the r_2 values for both the TA-USIONPs and QA-USIONPs are the same, however, the r_1 relaxivity for the QA-USIONPs was ~2.5 times lower than the r_1 of TA-USIONPs.

3.2. Cellular Uptake Studies. We first investigated if QA-USIONPs and TA-USIONPs affect cancer cell proliferation and viability. To test this, we performed a quantitative MTS cell proliferation assay. We found that both QA-USIONPs and TA-USIONPs do not significantly impact MDA-MB-231Br cellular proliferation (Figure 2). In addition, MDA-MB-231Br

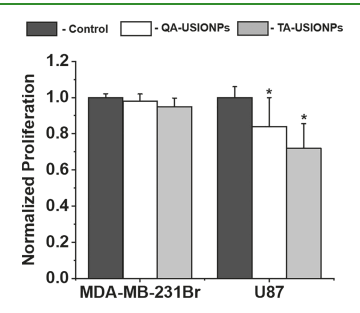


Figure 2. Proliferation of MDA-MB-231Br and U87 cells treated with $50 \mu g/mL$ of QA-USIONPs or TA-USIONPs for 72 h. Error bars represent standard deviation. N = 9 replicates per condition. *Indicates statistically significant difference (p < 0.05) compared to the respective control group.

cell viability was also unaffected by QA-USIONPs and TA-USIONPs (Figure S3). In case of U87 cells, we did observe significant (p < 0.05) decrease in cellular proliferation because of QA-USIONPs (by ~0.2-fold) and TA-USIONPs (by ~0.3fold) compared to nontreated control (Figure 2). However, U87 cell viability was unaffected by QA-USIONPs and TA-USIONPs (Figure S3). This indicates that the presence of QA-USIONPs and TA-USIONPs affects the cellular proliferation but not the viability in case of U87 cells. The cellular proliferation of MDA-MB-231Br cells was not affected by QA-USIONPs or TA-USIONPs treatment (Figure S4). However, the presence of QA-USIONPs and TA-USIONPs affected U87 cell proliferation in a dose-independent manner (Figure S5). Overall, these results indicate that the QA-USIONPs and TA-USIONPs tend to impact the cellular proliferation (depending on the cell line); however, they do not impact cell viability.

Next, we evaluated the targeting capabilities of QA-USIONPs and TA-USIONPs by characterizing their uptake by MDA-MB-231Br and U87 cancer cells. Qualitative Prussian blue staining revealed that the uptake of QA-USIONPs by both cell lines was higher compared to TA-USIONPs at any given time point (Figure 3A,B). QA-USIONPs were observed to localize near the cell membrane at early time points (i.e., 4 h) specifically in the case of MDA-MB-231Br cells (Figures 3A, S6), indicating interaction between QA-USIONPs and certain cell surface receptors.

To confirm the qualitative observations from the Prussian blue iron staining, we performed quantitative ferrozine colorimetric assay for determining the cellular iron content as described previously. 62 The calibration curve was generated through standard solutions of equal volumes as that of test samples ($R^2 = 0.99$) (Figure S7). While analyzing the ferrozine colorimetric assay data, all the data points were adjusted to accommodate for the inherent iron content in the control group (nontreated cells). In addition, for the 4 h time point, the iron content in some samples treated with TA-USIONPs turned out to be negative after adjusting for the inherent iron content. These negative data points were set to zero as they

represent the samples for which iron content was below the detection limit of the instrument.

Indeed, we observed significantly high cellular iron content in case of QA-USIONPs as compared to TA-USIONPs at any given time point for both cell lines consistent with Prussian blue staining results (Figure 4A,B). The cellular iron content in case of QA-USIONPs for MDA-MB-231Br was 7.6 \pm 3.06, 3.6 \pm 0.77, and 1.8 \pm 0.37 pg/cell at 4, 24, and 72 h, respectively, and for U87 was 7.1 ± 3.90 , 4.8 ± 0.34 , and 3.3 ± 1.56 pg/cell at 4, 24, and 72 h, respectively (Figure 4A,B). In case of TA-USIONPs, the cellular iron content for MDA-MB-231Br was 0.17 ± 0.33 , 0.73 ± 0.69 , and 0.45 ± 0.19 pg/cell at 4, 24, and 72 h, respectively, and for U87 was 0.60 ± 0.39 , 0.61 ± 0.09 , and 1.63 ± 0.05 pg/cell at 4, 24, and 72 h, respectively (Figure 4A,B). Further, the ratios of the magnitude of iron content in cells treated with TA-USIONPs to the magnitude of iron content in cells treated with QA-USIONPs at 4, 24, and 72 h time points were computed in order to examine the targeting capability of QA-USIONPs at the early time point. The ratio was lowest at 4 h time point indicating that the QA-USIONPs tend to selectively bind to the cancer cells before being uptaken through processes such as endocytosis, whereas the TA-USIONPs are nonselectively up-taken through processes such as endocytosis (Figures 4C, S8). As the time proceeds, the ratio increases as ultimately TA-USIONPs are also nonselectively up-taken through endocytosis (evident via TEM visualization of endocytosis, Figure S8). Further, the ratio at 4 h time point was lower for MDA-MB-231Br cells (0.04 \pm 0.08) when compared to U87 cells (0.12 \pm 0.12), indicating enhanced targeting capability of QA-USIONPs in case of MDA-MB-231Br cells; however, this difference did not reach statistical significance when analyzed via nonparametric Wilcoxon each pair test (p = 0.08). This observation is in line with the observations made through Prussian blue staining, wherein we observed localization of QA-USIONPs near the MDA-MB-231Br cell membrane (Figures 3A, S6). In addition, the cellular uptake of QA-USIONPs was enough to generate a detectable MRI signal (Figure S9).

In order to establish the targeting capability of QA-USIONPs through their interaction with cancer cell surface receptors, the cells were blocked with free QA prior to feeding QA-USIONPs. Further, the impact of blocking the potential cancer cell surface receptors with free QA on the cellular uptake of QA-USIONPs was determined using ferrozine colorimetric assay. MDA-MB-231Br cells were chosen for this study because of the enhanced targeting capability of QA-USIONPs as observed via Prussian blue iron staining and ferrozine colorimetric assay. We theoretically estimated the concentration of surface-bound QA in 50 µg/mL of QA-USIONPs to be \sim 32 μ g/mL. It was assumed that at any given time point, only half the surface area of QA-USIONPs was available to interact with the cell membrane, and hence, the effective concentration of surface-bound QA interacting with the cell membrane was $\sim 16 \mu g/mL$. Based on this estimation, the following concentrations of free QA were chosen to block MDA-MB-231Br cells in order to cover a wide range: 1.6, 16, and 160 μ g/mL. The cells were blocked with QA for 4 h prior to treating with QA-USIONPs. Ferrozine colorimetric assay was performed 24 h after treatment with QA-USIONPs in order to measure cellular uptake. The 24 h time point was chosen to minimize the cellular uptake of QA-USIONPs because of nonspecific endocytosis which may occur at later time points (72 h). In addition, the cellular iron content at 24 **ACS Applied Materials & Interfaces**

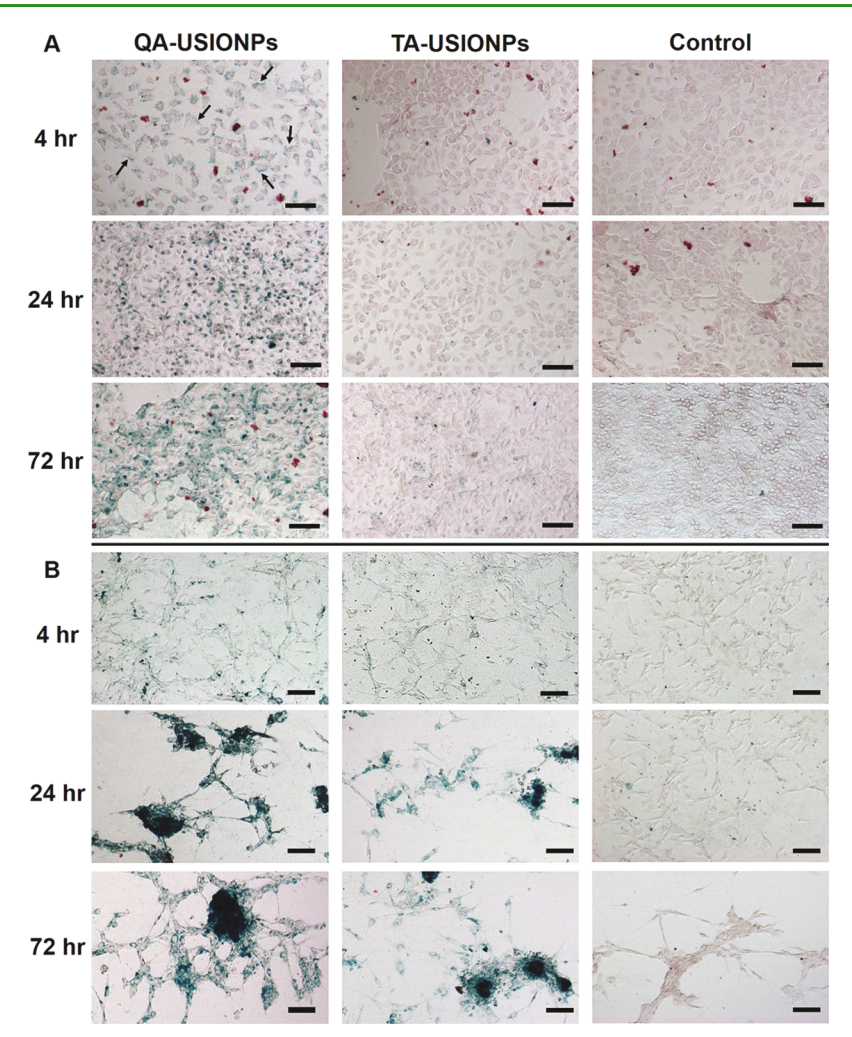


Figure 3. Prussian blue staining qualitatively reveals higher cellular uptake of QA-USIONPs when compared to TA-USIONPs at any given time-point for (A) MDA-MB-231Br and (B) U87 cells. Both the cell lines were treated with 50 μ g/mL of QA-USIONPs or TA-USIONPs for 4, 24 and 72 h following which Prussian blue staining was performed. Black arrows in case of 4 h time-point for MDA-MB-231Br cells treated with QA-USIONPs indicate the localization of QA-USIONPs near the cell membrane. Images were acquired at 10× magnification (scale bar = 100 μ m).

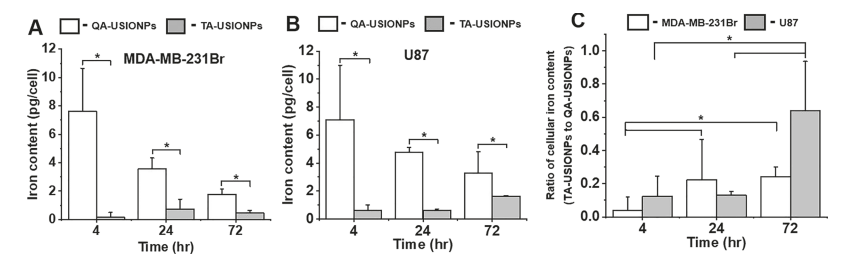


Figure 4. Quantification of cellular iron content by ferrozine colorimetric assay revealed significantly higher cellular uptake and targeting capability of QA-USIONPs when compared to TA-USIONPs at any given time-point. (A) Quantification of cellular iron content for MDA-MB-231Br cells treated with 50 μ g/mL of QA-USIONPs or TA-USIONPs for 4, 24 and 72 h, respectively. (B) Quantification of cellular iron content for U87 cells treated with 50 μ g/mL of QA-USIONPs or TA-USIONPs for 4, 24 and 72 h, respectively. (C) Ratio of the magnitude of iron content in cells treated with TA-USIONPs to the magnitude of iron content in cells treated with QA-USIONPs at 4, 24 and 72 h respectively for both MDA-MB-231Br and U87 cells. Error bars represent standard deviation. N = 6 replicates per condition. *Indicates statistically significant difference (p < 0.05).

h time point is also well above the detection limit so as to reliably compute the difference in the uptake due to blocking.

Indeed, we observed decreased (\sim 0.2-fold; p < 0.05) cellular uptake of QA-USIONPs by MDA-MB-231Br cells after blocking with free QA when compared to the nonblocked control group (Figure 5). This indicates that the QA coated onto the nanoparticles interacts with certain cell surface receptors conferring the QA-USIONPs with the targeting

capability. However, we observed that the decrease in the magnitude of cellular uptake of QA-USIONPs did not change significantly with the concentration of free QA used to block the cells. In addition, even the highest free QA concentration (i.e., $160~\mu g/mL$) was unable to completely block the uptake of QA-USIONPs. These observations may be attributed to the following reasons: (i) QA is a much smaller molecule and hence, after binding to the cell surface receptors, it might be

ACS Applied Materials & Interfaces

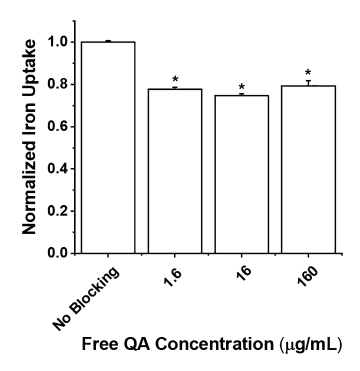


Figure 5. Blocking MDA-MB-231Br cells with free QA significantly decreases the cellular uptake of QA-USIONPs. MDA-MB-231Br cells were blocked with 1.6, 16 and 160 μ g/mL of free QA for 4 h prior to treating them with 50 μ g/mL of QA-USIONPs for next 24 h. Ferrozine colorimetric assay was performed to quantify the cellular iron content. Error bars represent standard deviation. N=6 replicates per condition. *Indicates statistically significant difference (p<0.05) compared to the non-blocked control group.

internalized and metabolized by the cell leaving the receptors free for QA-USIONPs to bind; ⁶⁶ (ii) free QA may not be able to block the binding site of the receptors completely (acting as a partial agonist), leaving room for the incoming QA-USIONPs to bind; (iii) possible differences in the binding affinity of free QA to P-selectin receptors compared to the surface bound QA in case of QA-USIONPs. ⁶⁷ Nonetheless, the significant decrease in the cellular uptake of QA-USIONPs after blocking with free QA indicates that the interaction of QA with certain cancer cell surface receptors may be mediating the selective uptake of QA-USIONPs and conferring them with the targeting capability.

3.3. Role of P-Selectin in Mediating the Selective Uptake of QA-USIONPs. To further investigate the role of cell receptors in mediating the selective uptake of QA-USIONPs by cancer cells, we treated cells with a P-selectin antibody and studied its impact on the cellular uptake of QA-USIONPs. We chose P-selectin because studies have reported the expression of P-selectin on the surface of tumor cells. 54–56 In particular, P-selectin has been shown to be overexpressed on

cancer cells in human cancer tissues including breast cancer⁵⁶ and GBM,55 whereas normal tissues exhibit minimal expression. In addition, overexpression of selectins in tumor and metastatic endothelium has been correlated to tumor invasiveness and metastasis as a result of increased tumor cellendothelium interactions and formation of tumor emboli. 56,58,59,68 Further, overexpression of selectins in the endothelium has also been associated with the formation of metastatic niche. 56,58-60 Because of these reasons, P-selectins have been investigated as a potential target for emerging targeted cancer therapeutics. 55,56,58 Also, selectins recognize and bind to the carbohydrate epitope sialyl lewisx (sLex), and hence, efforts have been made to chemically mimic the sLex. 52 Particularly, QA and its derivatives have been studied to mimic the sLex and target P-selectins for therapeutic purposes. 51,52,69 Recently, studies have demonstrated the E-/P-selectin mediated affinity of QA-conjugated polymeric nanoparticles toward tumor endothelium as a potential platform for targeted drug delivery. 57,70 In light of this information, we hypothesized that P-selectin could be mediating the selective uptake of QA-USIONPs by cancer cells.

To test this hypothesis, we first performed immunofluorescence staining to examine the expression of P-selectin in MDA-MB-231Br and U87 cells. Indeed, we observed that both cell lines express P-selectin; however, the expression was qualitatively higher in case of MDA-MB-231Br cells compared to the U87 cells (Figure 6). This observation is in line with that reported by Ferber et al., wherein they observed that the P-selectin gene is expressed variably in all cancer types; however, the P-selectin expression was lowest in GBM tumors compared to other cancer types. MDA-MB-231Br cells were chosen for further blocking studies because of the enhanced targeting capability of QA-USIONPs in case of these cells as established earlier and the higher expression of P-selectin noted as compared to U87 cells.

MDA-MB-231Br cells were blocked with the anti-P-selectin antibody at the concentration of 2.5 and 16 μ g/mL for 4 h before treating with QA-USIONPs. Similar to the free QA blocking study, ferrozine colorimetric assay was performed 24 h after treating with QA-USIONPs in order to measure cellular uptake. Indeed, we observed decreased (\sim 0.1-fold; p < 0.05)

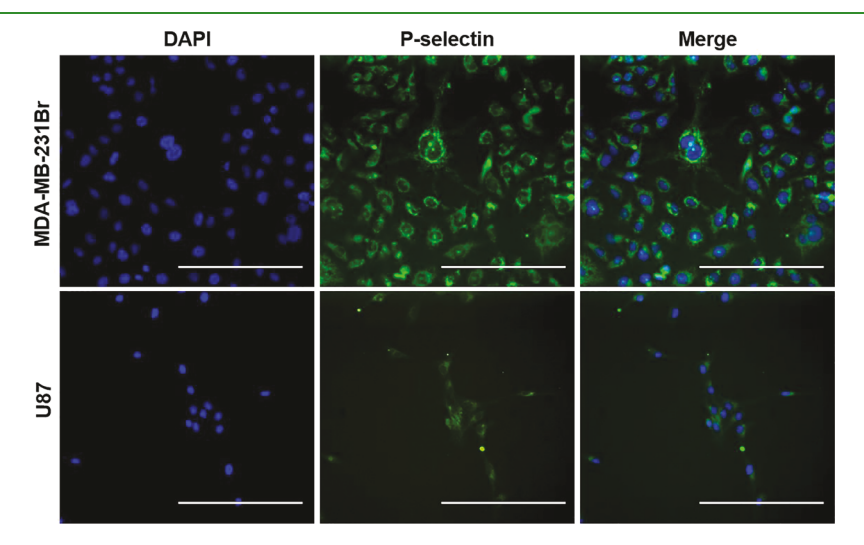


Figure 6. Immunofluorescence staining revealed relatively high expression of P-selectin in MDA-MB-231Br cells (upper panel) when compared to the U87 cells (lower panel). The images were taken at the same exposure time = 400 ms. Blue: DAPI nuclear stain and Green: P-selectin. Images were acquired at $20 \times$ magnification (scale bar = $200 \ \mu m$).

cellular uptake of QA-USIONPs by MDA-MB-231Br cells after blocking with the anti-P-selectin antibody when compared to the nonblocked control group (Figure 7). Similar to the free

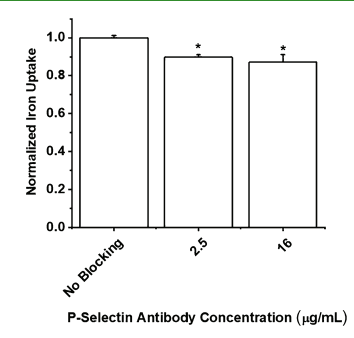


Figure 7. P-selectin receptor blocking significantly decreases the cellular uptake of QA-USIONPs by MDA-MB-231Br cells. MDA-MB-231Br cells were blocked with 2.5 and 16 μ g/mL anti-P-selectin antibody for 4 h prior to treating them with 50 μ g/mL of QA-USIONPs for next 24 h. Ferrozine colorimetric assay was performed to quantify the cellular iron content. Error bars represent standard deviation. N=6 replicates per condition. *Indicates statistically significant difference (p < 0.05) compared to the non-blocked control group.

QA blocking study, it was observed that the decrease in the magnitude of cellular uptake of QA-USIONPs did not change significantly with the concentration of the anti-P-selectin antibody. In addition, even the highest concentration of the blocking antibody (16 μ g/mL) was unable to completely block the uptake of QA-USIONPs. This may be due to QA-USIONPs binding to other cell surface receptors, particularly, other selectins such as E-selectin. Specifically, both P- and Eselectins are known to identify and bind to sLex which serves as the minimal carbohydrate epitope and bear similarities.⁵ The fact that QA and its derivatives have been widely investigated for mimicking sLex and given the similarities between selectins, it is plausible for QA-USIONPs to bind to other selectins and other existing cell surface receptors.⁵² Further, this might also be due to possible internalization of the anti-P-selectin antibody following its interaction with Pselectin receptors. In addition, the anti-P-selectin antibody utilized in the study was the monoclonal antibody (binding to only single epitope). However, there is a possibility that blocking with the polyclonal anti-P-selectin antibody could potentially result in further reduction in the uptake of QA-USIONPs as it would block multiple epitopes on the P-selectin receptor. Nonetheless, the blocking of P-selectin cell surface receptors led to a significant decrease in the cellular uptake of QA-USIONPs, establishing that the selective uptake of QA-USIONPs by MDA-MB-231Br cancer cells was, in part, mediated by P-selectin cell surface receptors.

4. CONCLUSIONS

In conclusion, we successfully synthesized QA-USIONPs for the first time and characterized their uptake by cancer cells in vitro. Using highly aggressive primary (U87) and metastatic (MDA-MB-231Br) brain cancer cells, we compared the in vitro cellular uptake of QA-USIONPs and previously reported TA-USIONPs, ^{50,61} revealing that these cancer cells selectively uptake QA-USIONPs. Further, for the first time, we established the role of the cell surface receptors; specifically, P-selectin in partly mediating the selective uptake of QA-

USIONPs by cancer cells. Given that studies have reported overexpression of P-selectin in tumor cells, \$4-56 tumor microenvironment, \$6,57 and at the metastatic niche, \$6,58-60 QA-USIONPs hold potential to be utilized as a platform for tumor-targeted drug delivery and in imaging and detection of primary and metastatic tumors. Future studies would investigate the tumor-site localization of QA-USIONPs in vivo for gaining more insights into their tumor-targeting capability.

ASSOCIATED CONTENT

S Supporting Information

The Supporting Information is available free of charge on the ACS Publications website at DOI: 10.1021/acsami.9b00606.

Sample preparation for TEM visualization of endocytosis; MRI sample preparation; high-resolution TEM images and particle size distribution of TA-USIONPs and QA-USIONPs; intensity and number distribution of TA-USIONPs and QA-USIONPs in culture media at 4, 24, and 72 h; cellular viability of MDA-MB-231Br and U87 cells treated with QA-USIONPs and TA-USIONPs; MDA-MB-231Br dose-dependent cellular proliferation for QA-USIONPs and TA-USIONPs; U87 dose-dependent cellular proliferation for QA-USIONPs and TA-USIONPs; enlarged Prussian blue staining images for MDA-MB-231Br cells treated with 50 μ g/mL of QA-USIONPs for 4, 24, and 72 h; calibration curve for the ferrozine colorimetric assay; TEM visualization of endocytosis; and MR images (PDF)

AUTHOR INFORMATION

Corresponding Authors

*E-mail: ybao@eng.ua.edu. Phone: +1 (205) 348-9869(Y.B.). *E-mail: srao3@eng.ua.edu; Phone: +1 (205) 348-6564(S.S.R.).

ORCID ®

Shreyas S. Rao: 0000-0001-7649-0171

Author Contributions

A.A.N. and J.A.S. contributed equally to the work.

Notes

The authors declare no competing financial interest.

■ ACKNOWLEDGMENTS

This work was supported by the University of Alabama start-up funds (to S.R.) and in part by the National Science Foundation (DMR 1149931 (Y.B.), CBET 1604677 (S.R.), and CBET 1749837 (S.R.)).

REFERENCES

- (1) Bao, Y.; Sherwood, J. A.; Sun, Z. Magnetic iron oxide nanoparticles as T1 contrast agents for magnetic resonance imaging. *J. Mater. Chem. C* **2018**, *6*, 1280–1290.
- (2) Okuhata, Y. Delivery of Diagnostic Agents for Magnetic Resonance Imaging. Adv. Drug Delivery Rev. 1999, 37, 121–137.
- (3) Rogosnitzky, M.; Branch, S. Gadolinium-Based Contrast Agent Toxicity: A Review of Known and Proposed Mechanisms. *BioMetals* **2016**, *29*, 365–376.
- (4) Wang, Y. X. Superparamagnetic Iron Oxide Based MRI Contrast Agents: Current Status of Clinical Application. *Quant. Imag. Med. Surg.* **2011**, *1*, 35–40.

- (5) Brisset, J.-C.; Sigovan, M.; Chauveau, F.; Riou, A.; Devillard, E.; Desestret, V.; Touret, M.; Nataf, S.; Honnorat, J.; Canet-Soulas, E.; Nighoghossian, N.; Berthezene, Y.; Wiart, M. Quantification of Iron-Labeled Cells with Positive Contrast in Mouse Brains. Mol. Imag. Biol. 2011, 13, 672-678.
- (6) Baiu, D. C.; Brazel, C. S.; Bao, Y.; Otto, M. Interactions of Iron Oxide Nanoparticles with the Immune System: Challenges and Opportunities for Their Use in Nano-Oncology. Curr. Pharm. Des. 2013, 19, 6606-6621.
- (7) Hamm, B.; Staks, T.; Taupitz, M.; Maibauer, R.; Speidel, A.; Huppertz, A.; Frenzel, T.; Lawaczeck, R.; Wolf, K. J.; Lange, L. Contrast-enhanced MR imaging of liver and spleen: First experience in humans with a new superparamagnetic iron oxide. J. Magn. Reson. Imaging 1994, 4, 659-668.
- (8) Macher, T.; Totenhagen, J.; Sherwood, J.; Qin, Y.; Gurler, D.; Bolding, M. S.; Bao, Y. Ultrathin Iron Oxide Nanowhiskers as Positive Contrast Agents for Magnetic Resonance Imaging. Adv. Funct. Mater. 2015, 25, 490-494.
- (9) Kim, B. H.; Lee, N.; Kim, H.; An, K.; Park, Y. I.; Choi, Y.; Shin, K.; Lee, Y.; Kwon, S. G.; Na, H. B.; Park, J.-G.; Ahn, T.-Y.; Kim, Y.-W.; Moon, W. K.; Choi, S. H.; Hyeon, T. Large-Scale Synthesis of Uniform and Extremely Small-Sized Iron Oxide Nanoparticles for High-ResolutionT1Magnetic Resonance Imaging Contrast Agents. J. Am. Chem. Soc. 2011, 133, 12624-12631.
- (10) Shen, Z.; Chen, T.; Ma, X.; Ren, W.; Zhou, Z.; Zhu, G.; Zhang, A.; Liu, Y.; Song, J.; Li, Z.; Ruan, H.; Fan, W.; Lin, L.; Munasinghe, J.; Chen, X.; Wu, A. Multifunctional Theranostic Nanoparticles Based on Exceedingly Small Magnetic Iron Oxide Nanoparticles for T1-Weighted Magnetic Resonance Imaging and Chemotherapy. ACS Nano 2017, 11, 10992-11004.
- (11) Verma, A.; Stellacci, F. Effect of Surface Properties on Nanoparticle-Cell Interactions. Small 2010, 6, 12-21.
- (12) Patil, U.; Adireddy, S.; Jaiswal, A.; Mandava, S.; Lee, B.; Chrisey, D. In vitro/in vivo Toxicity Evaluation and Quantification of Iron Oxide Nanoparticles. Int. J. Mol. Sci. 2015, 16, 24417-24450.
- (13) Nel, A. E.; Mädler, L.; Velegol, D.; Xia, T.; Hoek, E. M. V.; Somasundaran, P.; Klaessig, F.; Castranova, V.; Thompson, M. Understanding biophysicochemical interactions at the nano-bio interface. Nat. Mater. 2009, 8, 543-557.
- (14) Wang, T.; Jiang, X. Size-Dependent Stability of Water-Solubilized CdTe Quantum Dots and Their Uptake Mechanism by Live HeLa Cells. ACS Appl. Mater. Interfaces 2013, 5, 1190-1196.
- (15) Cheng, X.; Tian, X.; Wu, A.; Li, J.; Tian, J.; Chong, Y.; Chai, Z.; Zhao, Y.; Chen, C.; Ge, C. Protein Corona Influences Cellular Uptake of Gold Nanoparticles by Phagocytic and Nonphagocytic Cells in a Size-Dependent Manner. ACS Appl. Mater. Interfaces 2015, 7, 20568-
- (16) Untener, E. A.; Comfort, K. K.; Maurer, E. I.; Grabinski, C. M.; Comfort, D. A.; Hussain, S. M. Tannic Acid Coated Gold Nanorods Demonstrate a Distinctive Form of Endosomal Uptake and Unique Distribution within Cells. ACS Appl. Mater. Interfaces 2013, 5, 8366-8373.
- (17) Saikia, J.; Yazdimamaghani, M.; Hadipour Moghaddam, S. P.; Ghandehari, H. Differential Protein Adsorption and Cellular Uptake of Silica Nanoparticles Based on Size and Porosity. ACS Appl. Mater. Interfaces 2016, 8, 34820-34832.
- (18) Chithrani, B. D.; Ghazani, A. A.; Chan, W. C. W. Determining the Size and Shape Dependence of Gold Nanoparticle Uptake into Mammalian Cells. Nano Lett. 2006, 6, 662-668.
- (19) Chithrani, B. D.; Chan, W. C. W. Elucidating the Mechanism of Cellular Uptake and Removal of Protein-Coated Gold Nanoparticles of Different Sizes and Shapes. Nano Lett. 2007, 7, 1542-1550.
- (20) Jiang, W.; Kim, B. Y. S.; Rutka, J. T.; Chan, W. C. W. Nanoparticle-Mediated Cellular Response Is Size-Dependent. Nat. Nanotechnol. 2008, 3, 145-150.
- (21) Zhang, Y.; Tekobo, S.; Tu, Y.; Zhou, Q.; Jin, X.; Dergunov, S. A.; Pinkhassik, E.; Yan, B. Permission to Enter Cell by Shape: Nanodisk Vs Nanosphere. ACS Appl. Mater. Interfaces 2012, 4, 4099-4105.

- (22) Nguyen, T.-H.; Schuster, N.; Greinacher, A.; Aurich, K. Uptake Pathways of Protein-Coated Magnetic Nanoparticles in Platelets. ACS Appl. Mater. Interfaces 2018, 10, 28314-28321.
- (23) Weis, C.; Blank, F.; West, A.; Black, G.; Woodward, R. C.; Carroll, M. R. J.; Mainka, A.; Kartmann, R.; Brandl, A.; Bruns, H.; Hallam, E.; Shaw, J.; Murphy, J.; Teoh, W. Y.; Aifantis, K. E.; Amal, R.; House, M.; Pierre, T. S.; Fabry, B. Labeling of Cancer Cells with Magnetic Nanoparticles for Magnetic Resonance Imaging. Magn. Reson. Med. 2014, 71, 1896-1905.
- (24) Cole, A. J.; David, A. E.; Wang, J.; Galbán, C. J.; Hill, H. L.; Yang, V. C. Polyethylene Glycol Modified, Cross-Linked Starch-Coated Iron Oxide Nanoparticles for Enhanced Magnetic Tumor Targeting. Biomaterials 2011, 32, 2183-2193.
- (25) Xu, J.-K.; Zhang, F.-F.; Sun, J.-J.; Sheng, J.; Wang, F.; Sun, M. Bio and Nanomaterials Based on Fe3O4. Molecules 2014, 19, 21506-
- (26) Villanueva, A.; Cañete, M.; Roca, A. G.; Calero, M.; Veintemillas-Verdaguer, S.; Serna, C. J.; del Puerto Morales, M.; Miranda, R. The Influence of Surface Functionalization on the Enhanced Internalization of Magnetic Nanoparticles in Cancer Cells. Nanotechnology 2009, 20, 115103.
- (27) NDong, C.; Tate, J. A.; Kett, W. C.; Batra, J.; Demidenko, E.; Lewis, L. D.; Hoopes, P. J.; Gerngross, T. U.; Griswold, K. E. Tumor Cell Targeting by Iron Oxide Nanoparticles Is Dominated by Different Factors in vitro Versus in vivo. PLoS One 2015, 10, No. e0115636.
- (28) Artemov, D.; Mori, N.; Okollie, B.; Bhujwalla, Z. M. MR molecular imaging of the Her-2/neu receptor in breast cancer cells using targeted iron oxide nanoparticles. Magn. Reson. Med. 2003, 49,
- (29) Cheng, K.; Peng, S.; Xu, C.; Sun, S. Porous Hollow Fe3O4Nanoparticles for Targeted Delivery and Controlled Release of Cisplatin. J. Am. Chem. Soc. 2009, 131, 10637-10644.
- (30) Kikumori, T.; Kobayashi, T.; Sawaki, M.; Imai, T. Anti-Cancer Effect of Hyperthermia on Breast Cancer by Magnetite Nanoparticle-Loaded Anti-Her2 Immunoliposomes. Breast Canc. Res. Treat. 2009, 113, 435-441.
- (31) Ito, A.; Kuga, Y.; Honda, H.; Kikkawa, H.; Horiuchi, A.; Watanabe, Y.; Kobayashi, T. Magnetite Nanoparticle-Loaded Anti-Her2 Immunoliposomes for Combination of Antibody Therapy with Hyperthermia. Cancer Lett. 2004, 212, 167-175.
- (32) Yang, H.-M.; Park, C. W.; Woo, M.-A.; Kim, M. I.; Jo, Y. M.; Park, H. G.; Kim, J.-D. HER2/neu Antibody Conjugated Poly(amino acid)-Coated Iron Oxide Nanoparticles for Breast Cancer MR Imaging. Biomacromolecules 2010, 11, 2866-2872.
- (33) Mao, H.; Chen, H.; Wang, L.; Yu, Q.; Qian, W.; Tiwari, D.; Yi, H.; Wang, A. Y.; Huang, J.; Yang, L. Anti-HER2 Antibody and ScFvEGFR-conjugated Antifouling Magnetic Iron Oxide Nanoparticles for Targeting and Magnetic Resonance Imaging of Breast Cancer. Int. J. Nanomed. 2013, 8, 3781-3794.
- (34) Jang, M.; Yoon, Y. I.; Kwon, Y. S.; Yoon, T.-J.; Lee, H. J.; Hwang, S. I.; Yun, B. L.; Kim, S. M. Trastuzumab-Conjugated Liposome-Coated Fluorescent Magnetic Nanoparticles to Target Breast Cancer. Korean J. Radiol. 2014, 15, 411-422.
- (35) Hathaway, H. J.; Butler, K. S.; Adolphi, N. L.; Lovato, D. M.; Belfon, R.; Fegan, D.; Monson, T. C.; Trujillo, J. E.; Tessier, T. E.; Bryant, H. C.; Huber, D. L.; Larson, R. S.; Flynn, E. R. Detection of Breast Cancer Cells Using Targeted Magnetic Nanoparticles and Ultra-Sensitive Magnetic Field Sensors. Breast Canc. Res. 2011, 13,
- (36) Kievit, F. M.; Stephen, Z. R.; Veiseh, O.; Arami, H.; Wang, T.; Lai, V. P.; Park, J. O.; Ellenbogen, R. G.; Disis, M. L.; Zhang, M. Targeting of Primary Breast Cancers and Metastases in a Transgenic Mouse Model Using Rationally Designed Multifunctional SPIONs. ACS Nano 2012, 6, 2591-2601.
- (37) Ali, A. A. A.; Hsu, F.-T.; Hsieh, C.-L.; Shiau, C.-Y.; Chiang, C.-H.; Wei, Z.-H.; Chen, C.-Y.; Huang, H.-S. Erlotinib-Conjugated Iron Oxide Nanoparticles as a Smart Cancer-Targeted Theranostic Probe for MRI. Sci. Rep. 2016, 6, 36650.

- (38) Larson, T. A.; Bankson, J.; Aaron, J.; Sokolov, K. Hybrid Plasmonic Magnetic Nanoparticles as Molecular Specific Agents for MRI/Optical Imaging and Photothermal Therapy of Cancer Cells. *Nanotechnology* **2007**, *18*, 325101.
- (39) Gunduz, U.; Keskin, T.; Tansık, G.; Mutlu, P.; Yalcın, S.; Unsoy, G.; Yakar, A.; Khodadust, R.; Gunduz, G. Idarubicin-Loaded Folic Acid Conjugated Magnetic Nanoparticles as a Targetable Drug Delivery System for Breast Cancer. *Biomed. Pharmacother.* **2014**, *68*, 729–736.
- (40) Varshosaz, J.; Sadeghi-Aliabadi, H.; Ghasemi, S.; Behdadfar, B. Use of Magnetic Folate-Dextran-Retinoic Acid Micelles for Dual Targeting of Doxorubicin in Breast Cancer. *BioMed Res. Int.* **2013**, 2013, 680712.
- (41) Leuschner, C.; Kumar, C. S.; Hansel, W.; Soboyejo, W.; Zhou, J.; Hormes, J. Lhrh-Conjugated Magnetic Iron Oxide Nanoparticles for Detection of Breast Cancer Metastases. *Breast Canc. Res. Treat.* **2006**, *99*, 163–176.
- (42) Thomas, R. G.; Moon, M. J.; Lee, H.; Sasikala, A. R. K.; Kim, C. S.; Park, I.-K.; Jeong, Y. Y. Hyaluronic Acid Conjugated Superparamagnetic Iron Oxide Nanoparticle for Cancer Diagnosis and Hyperthermia Therapy. *Carbohydr. Polym.* **2015**, *131*, 439–446.
- (43) Chou, C.-P.; Chen, Y.-W.; Liou, G.-G.; Pan, H.-B.; Tseng, H.-H.; Hung, Y.-T. Specific Detection of CD133-positive Tumor Cells with Iron Oxide Nanoparticles Labeling Using Noninvasive Molecular Magnetic Resonance Imaging. *Int. J. Nanomed.* **2015**, *10*, 6997–7018.
- (44) Xu, Y.; Baiu, D. C.; Sherwood, J. A.; McElreath, M. R.; Qin, Y.; Lackey, K. H.; Otto, M.; Bao, Y. Linker-Free Conjugation and Specific Cell Targeting of Antibody Functionalized Iron-Oxide Nanoparticles. *J. Mater. Chem. B* **2014**, *2*, 6198–6206.
- (45) Thoidingjam, S.; Tiku, A. B. New Developments in Breast Cancer Therapy: Role of Iron Oxide Nanoparticles. *Adv. Nat. Sci.: Nanosci. Nanotechnol.* **2017**, *8*, 023002.
- (46) Xie, X.; Zhang, C. Controllable Assembly of Hydrophobic Superparamagnetic Iron Oxide Nanoparticle with mPEG-PLA Copolymer and its Effect on MR Transverse Relaxation Rate. *J. Nanomater.* **2011**, 2011, 152524.
- (47) Ai, H.; Flask, C.; Weinberg, B.; Shuai, X.-T.; Pagel, M. D.; Farrell, D.; Duerk, J.; Gao, J. Magnetite-Loaded Polymeric Micelles as Ultrasensitive Magnetic-Resonance Probes. *Adv. Mater.* **2005**, *17*, 1949–1952.
- (48) Nasongkla, N.; Bey, E.; Ren, J.; Ai, H.; Khemtong, C.; Guthi, J. S.; Chin, S.-F.; Sherry, A. D.; Boothman, D. A.; Gao, J. Multifunctional Polymeric Micelles as Cancer-Targeted, MRI-Ultrasensitive Drug Delivery Systems. *Nano Lett.* **2006**, *6*, 2427–2430.
- (49) Shapiro, E. M. Biodegradable, polymer encapsulated, metal oxide particles for MRI-based cell tracking. *Magn. Reson. Med.* **2015**, 73, 376–389.
- (50) Sherwood, J.; Lovas, K.; Rich, M.; Yin, Q.; Lackey, K.; Bolding, M. S.; Bao, Y. Shape-dependent cellular behaviors and relaxivity of iron oxide-based T1MRI contrast agents. *Nanoscale* **2016**, 8, 17506—17515.
- (51) Kaila, N.; Somers, W. S.; Thomas, B. E.; Thakker, P.; Janz, K.; DeBernardo, S.; Tam, S.; Moore, W. J.; Yang, R.; Wrona, W.; Bedard, P. W.; Crommie, D.; Keith, J. C.; Tsao, D. H. H.; Alvarez, J. C.; Ni, H.; Marchese, E.; Patton, J. T.; Magnani, J. L.; Camphausen, R. T. Quinic Acid Derivatives as Sialyl LewisX-Mimicking Selectin Inhibitors: Design, Synthesis, and Crystal Structure in Complex with E-selectin. *J. Med. Chem.* 2005, 48, 4346–4357.
- (52) Binder, F. P. C.; Ernst, B. E- and P-Selectin: Differences, Similarities and Implications for the Design of P-Selectin Antagonists. *Chimia Int. J. Chem.* **2011**, *65*, 210–213.
- (53) Girard, C.; Dourlat, J.; Savarin, A.; Surcin, C.; Leue, S.; Escriou, V.; Largeau, C.; Herscovici, J.; Scherman, D. Sialyl Lewisx analogs based on a quinic acid scaffold as the fucose mimic. *Bioorg. Med. Chem. Lett.* **2005**, *15*, 3224–3228.
- (54) Iwamura, T.; Caffrey, T. C.; Kitamura, N.; Yamanari, H.; Setoguchi, T.; Hollingsworth, M. A. P-selectin Expression in a Metastatic Pancreatic Tumor Cell Line (SUIT-2). *Cancer Res* **1997**, *57*, 1206–1212.

- (55) Ferber, S.; Tiram, G.; Sousa-Herves, A.; Eldar-Boock, A.; Krivitsky, A.; Scomparin, A.; Yeini, E.; Ofek, P.; Ben-Shushan, D.; Vossen, L. I.; Licha, K.; Grossman, R.; Ram, Z.; Henkin, J.; Ruppin, E.; Auslander, N.; Haag, R.; Calderón, M.; Satchi-Fainaro, R. Co-Targeting the Tumor Endothelium and P-selectin-Expressing Glioblastoma Cells Leads to a Remarkable Therapeutic Outcome. eLife 2017, 6, No. e25281.
- (56) Shamay, Y.; Elkabets, M.; Li, H.; Shah, J.; Brook, S.; Wang, F.; Adler, K.; Baut, E.; Scaltriti, M.; Jena, P. V.; Gardner, E. E.; Poirier, J. T.; Rudin, C. M.; Baselga, J.; Haimovitz-Friedman, A.; Heller, D. A. Pselectin Is a Nanotherapeutic Delivery Target in the Tumor Microenvironment. *Sci. Transl. Med.* **2016**, *8*, 345ra87.
- (57) Amoozgar, Z.; Park, J.; Lin, Q.; Weidle, J. H., III; Yeo, Y. Development of Quinic Acid-Conjugated Nanoparticles as a Drug Carrier to Solid Tumors. *Biomacromolecules* **2013**, *14*, 2389–2395.
- (58) Natoni, A.; Macauley, M. S.; O'Dwyer, M. E. Targeting Selectins and Their Ligands in Cancer. Front. Oncol. 2016, 6, 93.
- (59) Borsig, L. Selectins in Cancer Immunity. *Glycobiology* **2018**, 28, 648–655
- (60) Bendas, G.; Borsig, L. Cancer Cell Adhesion and Metastasis: Selectins, Integrins, and the Inhibitory Potential of Heparins. *Int. J. Cell Biol.* **2012**, *2012*, *676731*.
- (61) Sherwood, J.; Rich, M.; Lovas, K.; Warram, J.; Bolding, M. S.; Bao, Y. T1-Enhanced MRI-visible nanoclusters for imaging-guided drug delivery. *Nanoscale* **2017**, *9*, 11785–11792.
- (62) Riemer, J.; Hoepken, H. H.; Czerwinska, H.; Robinson, S. R.; Dringen, R. Colorimetric Ferrozine-Based Assay for the Quantitation of Iron in Cultured Cells. *Anal. Biochem.* **2004**, *331*, *370*–*375*.
- (63) Jadin, L.; Pastorino, S.; Symons, R.; Nomura, N.; Jiang, P.; Juarez, T.; Makale, M.; Kesari, S. Hyaluronan Expression in Primary and Secondary Brain Tumors. *Ann. Transl. Med.* **2015**, *3*, 80.
- (64) Sileika, T. S.; Barrett, D. G.; Zhang, R.; Lau, K. H. A.; Messersmith, P. B. Colorless Multifunctional Coatings Inspired by Polyphenols Found in Tea, Chocolate, and Wine. *Angew. Chem., Int. Ed.* **2013**, *52*, 10766–10770.
- (65) Sahiner, N.; Sagbas, S.; Aktas, N. Single Step Natural Poly(Tannic Acid) Particle Preparation as Multitalented Biomaterial. *Mater. Sci. Eng. C* **2015**, *49*, 824–834.
- (66) Hymel, D.; Peterson, B. R. Synthetic Cell Surface Receptors for Delivery of Therapeutics and Probes. *Adv. Drug Delivery Rev.* **2012**, 64, 797–810.
- (67) Yin, L.; Yang, Y.; Wang, S.; Wang, W.; Zhang, S.; Tao, N. Measuring Binding Kinetics of Antibody-Conjugated Gold Nanoparticles with Intact Cells. *Small* **2015**, *11*, 3782–3788.
- (68) Kim, Y. J.; Borsig, L.; Varki, N. M.; Varki, A. P-selectin Deficiency Attenuates Tumor Growth and Metastasis. *Proc. Natl. Acad. Sci. U.S.A.* **1998**, 95, 9325–9330.
- (69) Kaila, N.; Thomas Iv, B. E. Design and synthesis of sialyl Lewisx mimics as E- and P-selectin inhibitors. *Med. Res. Rev.* **2002**, 22, 566–601
- (70) Xu, J.; Lee, S. S.-Y.; Seo, H.; Pang, L.; Jun, Y.; Zhang, R. Y.; Zhang, Z. Y.; Kim, P.; Lee, W.; Kron, S. J.; Yeo, Y. Quinic Acid-Conjugated Nanoparticles Enhance Drug Delivery to Solid Tumors via Interactions with Endothelial Selectins. *Small* **2018**, *14*, 1803601.